

Externally-driven plasma models as candidates for pulsar radio emission

Sk. Minhajur Rahaman^{1*}, Dipanjan Mitra^{1,2}, George I. Melikidze^{2,3}

¹ National Centre for Radio Astrophysics, Tata Institute of Fundamental Research, Post Bag 3, Ganeshkind, Pune-411007, India

² Janusz Gil Institute of Astronomy, University of Zielona Góra, ul Szafrana 2, 65-516 Zielona Góra, Poland

³ Evgeni Kharadze Georgian National Astrophysical Observatory, 0301, Abastumani, Georgia

Accepted XXX. Received YYY; in original form ZZZ

ABSTRACT

Coherent radio emission from pulsars originates from excited plasma waves in an ultra-relativistic and strongly magnetized electron-positron pair plasma streaming along the open magnetic field lines of the pulsar. Traditional coherent radio emission models have relied on instabilities in this pair plasma. Recently alternative models have been suggested. These models appeal to direct coupling of the external electromagnetic field to the superluminal O-mode (lt_2 mode) during the time-dependent pair cascade process at the polar gap. The objective of this work is to provide generic constraints on plasma models based on lt_2 mode using realistic pulsar parameters. We find that the very short timescale associated with pair cascades does not allow lt_2 mode to be excited at radio frequencies and the impulsive energy transfer can only increase the kinetic spread (“temperature”) of the pair plasma particles. Moreover, under homogeneous plasma conditions, plasma waves on both branches of O-mode (i.e. superluminal lt_2 and subluminal lt_1) cannot escape the plasma. In the strongly magnetized pair plasma, only the extraordinary mode (t mode) can escape freely. We show that any generic fictitious mechanisms does not result in the wave electric field of t mode to have predominant orientation either parallel or perpendicular to the magnetic field plane as observed. Such fictitious mechanisms will inevitably lead to depolarization of signals and cannot account for the highly polarized single pulses observed in pulsars. We suggest coherent curvature radiation as a promising candidate for pulsar radio emission mechanism.

Key words: pulsars – non-thermal – waves

1 INTRODUCTION

The coherent radio emission from pulsars is believed to originate from an electron-positron pair plasma that streams relativistically outward along the the open ambient magnetic field lines of the pulsar magnetosphere. Traditional models of coherent radio emission appeal to instabilities in this strongly magnetized and highly relativistic pair plasma. Such instability driven mechanisms are broadly divided into two classes viz., maser and antenna mechanisms (Ginzburg & Zhelezniakov 1975; Melrose 1995). The former assumes that radio emission is generated by certain types of plasma instabilities that generate plasma waves capable of escaping the magnetosphere, while the latter relies on coherent curvature radiation as the main source of the observed radio waves. Recently a class of externally driven models have been proposed that avoids the need for plasma instability (Philippov et al. 2020 hereafter PTS20 ; Melrose et al. 2021; Cruz et al. 2021).

The preferred mechanism of pulsar radio emission should explain the essential characteristics of the observed radio emission. Current observations tightly constrains the location of the pulsar radio emission to be far inside the magnetosphere, at least below 10% of the light cylinder (Blaskiewicz et al. 1991; Mitra 2017). In this region most of plasma instabilities are suppressed by the strong dipolar ambient magnetic field of the pulsar. The only instability that can develop is the two-stream instability which assumes wave-particle in-

teraction at the Cherenkov plasma resonance. As the magnetic field strength gets weaker with distance, nearer the light cylinder some other instabilities like cyclotron and/or Cherenkov-curvature drift instabilities can also develop (e.g. Kazbegi et al. 1991; Lyutikov et al. 1999). These instabilities are of the maser kind, and given the emission height constraint they can be ruled out as possible candidates for pulsar radio emission.

In addition to the location of the radio emission zone, polarisation of the observed radiation provides an important constraint. The observed radio waves are highly linearly polarised and the polarisation vector is either parallel or perpendicular to the plane in which the dipolar magnetic field lines lie (Melikidze et al. 2014 ; Mitra et al. 2009; Lai et al. 2001). Therefore, any pulsar radio-emission mechanism(s) should be based on excitation of eigen modes of the strongly magnetised electron-positron pair plasma which can propagate in the magnetosphere and then escape from it by preserving the observed polarization features.

The eigen modes in strongly magnetized homogeneous pair plasma has been extensively studied (e.g. Hardee & Rose 1978; Arons & Barnard 1986). Here we briefly summarize the behaviour of the eigen modes as discussed in Shapakhidze et al. (2003). Generally, there are two eigen modes in magnetised pair plasma, the so called ordinary (O-mode or lt mode) and extraordinary (t mode) modes. The wave electric field (also referred as polarisation vector) of O-mode lies in the plane of the wave vector \vec{k} and the ambient magnetic field \vec{B} and has a component along the ambient magnetic field. The t mode always has a purely transverse nature and

* E-mail: rahaman@ncra.tifr.res.in

its polarization vector is directed perpendicular to \vec{k} and \vec{B} plane. The O-mode represent longitudinal-transverse waves and have two branches, one subluminal lt_1 -mode and the other superluminal lt_2 -mode. In the case of strictly parallel propagation (with respect to the external magnetic field) the superluminal branch coincides with the Langmuir wave and is purely longitudinal. For larger angles the superluminal lt_2 -mode has longitudinal-transverse nature.

When propagating along the magnetic field, lt_1 -mode is an arbitrarily polarized purely transverse wave, whereas for oblique propagation it becomes a longitudinal-transverse wave. The phase velocity of lt_1 -mode is always subluminal while lt_2 -mode is superluminal at frequencies smaller than the characteristic frequency ω_1 (where the mode touches the kc line, see equation 6 defined later) and subluminal at frequencies above ω_1 . The dispersion relation of the t mode at radio frequencies has one subluminal branch which is always transverse nature. This mode is called the t -mode. Let us underline that polarisation vectors of linearly polarized X-and O-modes are defined by the plane of \vec{k} and the local magnetic field \vec{B} , while the polarisation vector of observed radio waves are parallel or perpendicular to the plane of curved dipolar field lines. Therefore, any preferred emission mechanism should address the problem of how the linear polarization of the plasma X and O-mode emerges from the plasma as electromagnetic waves with the observed polarization direction. In the rest of the paper when O-mode is mentioned it stands for combined lt_1 and lt_2 mode, and the X mode stands for the t mode.

Several theoretical studies (Asseo & Melikidze 1998; Melikidze et al. 2000; Gil et al. 2004; Lakoba et al. 2018; Rahaman et al. 2020) demonstrate that the observational constraints of pulsar radio emission location and linear polarization can be explained by coherent curvature radiation (CCR) due to motion of charge bunches along curved magnetic field lines. Curvature radiation has the feature that the radiation is predominantly polarized in the magnetic field plane of the particle trajectory and a fraction is polarized perpendicular to the plane (Jackson 1999). In strongly magnetized plasma CCR due to charge bunch can excite the t and lt_1 mode, and since curvature radiation mechanism can distinguish the magnetic field line planes the excited t and lt_1 mode has its polarization perpendicular and parallel to the magnetic field line planes respectively. The t mode has vacuum like character and can escape freely with its polarization being perpendicular to the magnetic field line planes. The lt_1 mode has polarization in the plane of the magnetic field and cannot easily escape from the plasma. Thus the CCR theory still has difficulty in explaining the emergence of polarization mode that lies parallel to the magnetic field line planes (see Melikidze et al. 2014; hereafter MMG14).

Recently PTS20 proposed that the lt_2 -mode can be a candidate for pulsar radio emission. They demonstrate via particle-in-cell simulations that due to the time dependent and non-uniform pair creation process across the magnetic field lines in the vacuum gap, the induced electric field in the vacuum gap is screened accompanied by emission of waves which are electromagnetic in nature. The electromagnetic waves have superluminal phase velocity and PTS20 suggests that these waves be identified with the lt_2 mode of the plasma, and as the density in the plasma decreases with height, the waves can decouple from the plasma as electromagnetic radiation. However, these suggestions needs to be demonstrated and the purpose of this is to investigate if the lt_2 mode can be a candidate for the observed pulsar radio emission.

The organization of the paper is as follows. Section 2 gives a summary of the observational constraints of pulsar radio emission. In Section 3 the properties of O-mode are reviewed. In Section 4 the condition required for the validity of the dispersion relation are es-

Table 1. Typical multiplicity (κ) of pair plasma, radius of curvature (ρ_c), the ratio $b = B_s/B_d$ for different magnetic topology at the neutron star surface.

Quantity	Dipolar	Non-dipolar
κ	$10 - 10^2$	$10^4 - 10^5$
ρ_c (in cm)	10^8	10^5
b	1	$10 - 10^2$

tablished. In Section 5 the linear polarization features of the escaping wave (t -mode) from pulsar plasma are established for an arbitrary fictitious mechanism and contrasted with CCR. Our findings are summarized in Section 6.

2 OBSERVATIONAL CONSTRAINTS OF PULSAR RADIO EMISSION

In this section we briefly summarise the observational and theoretical inputs that constrains the parameter space of pulsar plasma.

- **Location of Radio Emission region, and the direction of emergent radio waves:** Most normal pulsars (defined as pulsars with periods P longer than about 50 milliseconds) are highly linearly polarized and the linear polarization position angle (PPA) across the pulse follows a characteristic S-shaped curve. This PPA behaviour can be explained by the rotating vector model (RVM, Radhakrishnan & Cooke 1969) according to which the linear polarization vector traces the change in the dipolar magnetic field line planes as the pulsar radio emission beam sweeps past the line of sight of the observer. As per the RVM the steepest gradient (SG) or inflexion point of the PPA traverse is associated with the fiducial magnetic field plane. In several pulsars two parallel PPA tracks following the RVM are seen. These tracks are separated by about 90° , and is commonly known as orthogonal polarization modes (OPM).

If the radio emission arises close to the neutron star surface then due to the effects of aberration and retardation the center of the total intensity pulse profile leads the SG point by a certain amount depending on the radio emission height. This effect is observed in several normal pulsars and the radio emission heights is constrained to be a few hundred km above the neutron star surface, or below 10% of the light cylinder radius (von Hoensbroech & Xilouris 1997; Blaskiewicz et al. 1991; Mitra & Li 2004; Weltevredre & Johnston 2008; Mitra 2017; Pétri & Mitra 2020).

Further, observations can constrain the direction of the emerging polarization with respect to the dipolar magnetic field planes of the pulsar. In the case of the Vela pulsar using a combination of X-ray image of the pulsar wind nebula and radio polarization Lai et al. (2001) found that the emerging radiation is perpendicular to the magnetic field line planes. For several other pulsars, by measuring the absolute PPA and the direction of the absolute proper motion PM, the quantity $|\text{PM-PPA}|$ shows a distribution around 0° and 90° (see e.g. Johnston et al. 2005; Noutsos et al. 2013, 2012; Rankin 2015; Force et al. 2015). These observations are interpreted as evidence for the emerging electric field being either parallel or perpendicular to the magnetic field line planes that correspond to the OPM's.

- **Highly polarized single pulses:** Average pulse profiles are formed by averaging hundred to thousands of single pulses, during which it can average out the short timescale features that govern the

pulsar emission mechanism. Characterization of single pulses are hence more useful to obtain constraints for pulsar emission mechanism. Single pulses from normal pulsars are composed of sub-pulses and often the subpulses are observed to be highly polarized, sometimes being linearly polarized close to 100%. [Mitra et al. \(2009\)](#) showed that when such highly polarized subpulses are seen, their underlying PPA follow the RVM of the average profile. Further MMG14 showed that these kind of highly polarized subpulses are associated with both the OPM in pulsars. These highly polarized pulses are free from magnetospheric depolarization effects, and since they follow the RVM, their polarization direction are parallel or perpendicular to the magnetic field planes. Thus, any radio emission mechanism should be able to predict the features of highly polarized single pulses.

• **Constraints on surface magnetic field and particle flow** The pulsar radio emission is broadband in nature and arises from regions of open dipolar ambient magnetic field lines located a few hundred km above the neutron star surface ([Mitra & Li 2004](#)). However, several lines of evidence suggest the presence of strong non-dipolar surface magnetic fields at the polar cap region. For example radio emission from the long period pulsar J2144-3933 ([Young et al. 1999](#)), can only be explained by efficient pair creation process which can be achieved by strong multipolar surface magnetic field (see [Gil & Mitra 2001](#); [Mitra et al. 2020](#)). Also the single pulse phenomenon of subpulse drifting show significant variety which can only be explained by invoking surface multipolar magnetic fields ([Ruderman & Sutherland 1975](#); [Basu et al. 2020](#)). Combined radio and X-ray observations can also constrain the surface magnetic fields. The sparking discharges due to pair creation at the polar cap gives rise to a backflow of accelerated charges which bombard the polar cap. This heats the polar cap (with radius r_p) up to a temperature $T \sim$ few million kelvin and it starts emitting thermal X-rays. The X-ray luminosity provides an estimate of the size of the polar cap ($L_X = \sigma T^4 \times \pi r_p^2$). X-ray studies for normal period radio pulsars have consistently found the polar cap sizes to be smaller than expected from a purely dipolar magnetic field at the polar cap. Using flux conservation argument, the strength of the magnetic field at the neutron star surface has been found to be around ten to hundred times stronger than the the global dipole field (Table 1 of [Geppert 2017](#)). Besides, recent studies like that of [Riley et al. 2019](#) have found evidence of non-dipolar surface magnetic field on millisecond pulsars. In several pulsars there is a phase off-set between the pulsed thermal X-ray hotspot emission from polar cap and the radio pulse. This phase off-set is larger than that is expected from a magnetic field topology which retains its dipolar character right up to the surface. The presence of strong multipolar surface magnetic fields need to be invoked to explain this phase offset (see [Szary et al. 2017](#); [Arumugasamy & Mitra 2019](#); [Pétri & Mitra 2020](#)).

Another consequence of the presence of non-dipolar surface magnetic field is that it enables efficient pair creation, and as a result a high density plasma pulsar wind is produced. Studies of pulsar wind nebula (see [de Jager 2007](#); [Blasi & Amato 2011](#)) has been used to constrain the density of the plasma, and it is found that the density is about $10^4 - 10^5$ times more than the corotational Goldreich-Julian density n_{GJ} ([Goldreich & Julian 1969](#)).

The evidence above suggests although the surface magnetic field has a highly non-dipolar character, the higher order magnetic moments of this configuration rapidly decays with distance such that only the dipolar topology exists at the radio emission zone. This behaviour can be understood in terms of the model by [Gil et al. 2002](#) (hereafter GMM02). In this model, the surface magnetic field is modelled as

Table 2. Limiting values at the cut-off frequency ω_o and the characteristic plasma frequency ω_1 for lt_2 mode for parallel refractive index n_{\parallel} , the dimensionless variable χ^2 and the group velocity \vec{v}_g . Here, ϑ is the angle between \vec{k} and \vec{B} , and Θ is the angle between the wave electric field \vec{E}_{wave} and the wave vector \vec{k} . The unit vector \hat{b}_{\parallel} and \hat{b}_{\perp} are directed along and perpendicular to the ambient magnetic field \vec{B} respectively.

Quantity	$\omega \rightarrow \omega_o$	$\omega \rightarrow \omega_1$
n_{\parallel}	0	$\sqrt{1 - n_{\perp}^2}$
χ^2	$1 - n_{\perp}^2$	0
\vec{v}_g/c	$(1 - n_{\perp}^2)\beta_o \hat{b}_{\parallel} + n_{\perp} \hat{b}_{\perp}$	$n_{\parallel} \hat{b}_{\parallel} + n_{\perp} \hat{b}_{\perp}$
Θ	ϑ	$\pi/2 - \vartheta$

a superposition of a global dipole field (B_d) and a crust-anchored local field ($B_s = bB_d$) where $b \sim 10 - 100$ such that the magnetic moment of crust-anchored field μ_m is much lower than the magnetic moment of the global field μ_d . The contribution due to the crust-anchored field rapidly decays with distance from the neutron star such that by around 10 km above the surface the ambient magnetic field topology is completely dipolar (see fig. 2 of GMM02). In this model, the field line curvature ρ_c at the surface is dictated by the local field whereas the the field line curvature ρ_c at the radio emission region is dictated by the global field.

Copious pair plasma in pulsars are produced near the pulsar polar cap where an inner accelerating region with strong unscreened electric field exists ([Ruderman & Sutherland 1975](#)). In this region high energy photons undergo magnetic pair creation, and a high energy primary beam relativistically moving outwards with lorentz factors of $\sim 10^6$ can be produced. This beam can further radiate in curved magnetic field resulting in pair cascade, which leads to the production of the dense pair plasma having lorentz factors of about $\sim 10^2$. The number density of the pair plasma n_s exceeds the co-rotational density by a multiplicity factor κ ([Sturrock 1971](#)), i.e. $n_s = \kappa n_{GJ}$. Let us note that pair cascade simulations ([Arendt & Eilek 2002](#); [Hibschman & Arons 2001](#); [Medin & Lai 2007](#); [Szary et al. 2015](#); [Timokhin & Harding 2019](#)) show that smaller value of ρ_c on the surface increases the pair multiplicity and vice versa. A representative value for the multiplicity and the field line curvature are shown in Table 1.

In terms of pulsar parameters for a neutron star of radius R_{NS} the co-rotational number density at a radio emission height r is $n_{GJ} \sim 7 \times 10^{10} (P_{-15}/P)^{0.5} (R_{NS}/r)^3 \text{ cm}^{-3}$ where P is the pulsar period in seconds and P_{-15} is the spin-down rate normalized to 10^{-15} seconds per second. The plasma frequency is $\omega_p = \sqrt{4\pi n_s e^2/m_e}$ and can be written as,

$$\omega_p = 10^{10} \left(\frac{\kappa}{10^5} \right)^{1/2} \left(\frac{\dot{P}_{-15}}{P} \right)^{1/4} \left(\frac{500 \text{ km}}{r} \right)^{3/2} \text{ rad s}^{-1} \quad (1)$$

For typical pulsar parameters $r = 500 \text{ km}$, $\kappa = 10^5$, $P = 1 \text{ s}$, $\dot{P}_{-15} = 1$, and $R_{NS} = 10 \text{ km}$ the values are $n_{GJ} \sim 5.5 \times 10^5 \text{ cm}^{-3}$, $n_s \sim 5.5 \times 10^{10} \text{ cm}^{-3}$ and $\omega_p \sim 10^{10} \text{ rad s}^{-1}$.

3 PROPERTIES OF lt_2 MODE IN STRONG AMBIENT MAGNETIC FIELD

The region close to the neutron star from where the pulsar radio emission originates, the ratio of the plasma frequency to the

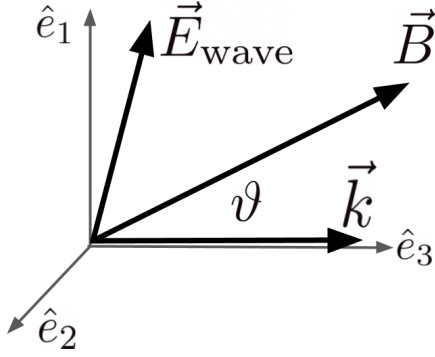


Figure 1. Cartesian co-ordinate system ($\hat{e}_1, \hat{e}_2, \hat{e}_3$) adopted from Kazbegi et al. 1991. The wave vector \vec{k} is taken along \hat{e}_3 . The angle between the wave vector \vec{k} and the dipolar ambient pulsar magnetic field \vec{B} is ϑ . The $k - B$ plane is confined to $\hat{e}_1 - \hat{e}_3$ plane. The electric field of the lt_2 waves is confined to the $k - B$ plane.

cyclotron frequency in terms of pulsar parameters is, $\omega_p/\omega_B = 2 \times 10^{-4} \times \kappa^{0.5} \mathfrak{R}^{1.5} \left(P^3/\dot{P}_{15} \right)^{0.25} \ll 1$, where $\mathfrak{R} = r/R_{LC}$ is the ratio of emission height r to the light-cylinder radius R_{LC} . Under such condition the approximation of pair plasma in infinite magnetic field is valid and the plasma flow can be assumed to be strictly one-dimensional. The corresponding dispersion relation of the O-mode of the homogeneous pair plasma in the observer frame of reference (hereafter OFR), is given by (see Eq. 48 of Arons & Barnard 1986)

$$(\omega^2 - k_{\parallel}^2 c^2) \left[1 - \frac{1}{2} \sum_{\alpha} \omega_{p\alpha}^2 \int_{-\infty}^{+\infty} dp \frac{f_{\alpha}^{(0)}}{\gamma^3 (\omega - k_{\parallel} v)^2} \right] - c^2 k_{\perp}^2 = 0 \quad (2)$$

where the index α denotes the electron and the positron distribution functions in the plasma. Here k_{\parallel} and k_{\perp} denote components of the wave vector \vec{k} parallel and perpendicular to the ambient pulsar magnetic field \vec{B} . For simplicity we can use the cold-plasma approximation, where the particle distribution functions can be replaced by delta-functions. Additionally, we assume the electron and the positron distribution functions to be co-incident. All plasma particles are assumed to move with the Lorentz factor γ_s . Under these simplifying assumptions, the dispersion relation of the O-mode as given by equation (2) reduces to the form

$$(\omega^2 - k_{\parallel}^2 c^2) \left[1 - \frac{\omega_p^2}{\gamma_s^3 (\omega - k_{\parallel} v_o)^2} \right] - k_{\perp}^2 c^2 = 0 \quad (3)$$

where $v_o/c = \beta_o = (1 - 1/\gamma_s^2)^{0.5}$. The above equation has two branches, and the lt_1 mode correspond to the case $\omega/k < c$ and lt_2 mode for which $\omega/k > c$.

To describe the waves we adopt co-ordinate system by Kazbegi et al. (1991) as shown in Fig.1, where the unit vectors \hat{e}_1, \hat{e}_2 and \hat{e}_3 are orthogonal to each other. The wave vector \vec{k} is along \hat{e}_3 and the ambient pulsar magnetic field \vec{B} lies in the $\hat{e}_1 - \hat{e}_3$ plane. The electric field \vec{E}_{wave} of the O-mode lies in the $k - B$ plane. The components of \vec{E}_{wave} parallel and perpendicular to the wave vector (\vec{k}) is E_3 and E_1 respectively. If Θ is the angle that the wave electric field of O-mode makes with the wave vector \vec{k} we have,

$$\tan \Theta = \frac{E_1}{E_3} \quad (4)$$

The electric field (E_2) of the t-mode is along \hat{e}_2 . For an angle ϑ between the wave vector \vec{k} and the ambient pulsar magnetic field \vec{B} , the components of \vec{k} along and perpendicular to \vec{B} are represented as $k_{\parallel} = k \cos \vartheta$ and $k_{\perp} = k \sin \vartheta$, such that the parallel and perpendicular refractive index can be defined as $n_{\parallel} = k_{\parallel} c/\omega$ and $n_{\perp} = k_{\perp} c/\omega$ respectively¹. A plasma wave of frequency ω can escape from the plasma only if the waves achieve vacuum-like propagation ($\omega = kc$) so as not to suffer refraction, acquire a transverse character ($E_3 = 0$) so as to acquire electromagnetic character, and is perpendicular to the ambient magnetic field ($E_{\parallel} = 0$) so as not to set up any plasma current along \vec{B} so as to decouple from the plasma particles. The t-mode has $\omega = kc$ for all $\omega \ll \omega_B$. Besides, since E_2 is perpendicular to the $k - B$ plane, t-mode automatically satisfies $E_3 = 0$ and $E_{\parallel} = 0$. Thus, t-mode can freely escape from the plasma at the broadband radio frequencies.

For strictly parallel propagation ($\vartheta = 0$), the lt_2 mode admits the purely longitudinal Langmuir (L) mode. The \vec{E}_{wave} of the L mode is directed along the \vec{k} viz., $E_1 = 0$. Two characteristic frequencies can be obtained from the dispersion relation of the L mode. First, the L-mode has a cut-off frequency ω_o at the long wavelength limit ($k \rightarrow 0$) given by

$$\omega_o = \frac{\omega_p}{\gamma_s^{3/2}} \quad (5)$$

Secondly, a characteristic plasma frequency can be identified where the L-mode touches the $\omega = kc$ line given by

$$\omega_1 = 2\omega_p \sqrt{\gamma_s} \quad (6)$$

For strictly perpendicular propagation ($\vartheta = \pi/2$), the lt_2 admits the purely transverse and electromagnetic TE mode. The TE mode has the same cut-off frequency ω_o as the L-mode and the mode remains superluminal for all frequencies $\omega > \omega_o$. The \vec{E}_{wave} of the TE mode is aligned along the ambient magnetic field \vec{B} with $E_{\parallel} = E_3 \neq 0$. Hence, even the purely transverse TE mode cannot escape from the plasma.

For any intermediate angle $0 < \vartheta < \pi/2$, the lt_2 mode has a cut-off frequency at ω_o and the longitudinal component of the electric field along the wave vector (E_3) dominates for frequencies near cut-off. The situation changes at higher frequencies, where the perpendicular component E_1 dominates. Thus, an important feature of the lt_2 -mode is that ratio of longitudinal and transverse E_1/E_3 which depends on the angle ϑ between the local magnetic field \vec{B} and \vec{k} . With increase of ϑ the transverse components increase, but at the same time the phase velocity also increases and the branch stays in superluminal area. This could be changed if ω_p/ω_B is near to unity, but this condition never can be reached in the pulsar magnetosphere (see Eq. 1 of MMG14).

In pulsar plasma, owing to the ultra-relativistic nature of the plasma particles excitation angles are generally considered to be small, as they are comparable to $1/\gamma_s$ beam of the plasma particles, thus $\vartheta \approx 1/\gamma_s \sim 0.01$ rad, (using $\gamma_s = 100$).

3.1 The dispersion curves and escape of lt_2 mode at small ϑ

Note that equation (3) can be arranged to give the form

¹ Note that the difference between the subscripts 1 – 3 that refers to components with respect to wave vector \vec{k} and the \parallel, \perp that refers to components with respect to the ambient pulsar magnetic field \vec{B} .

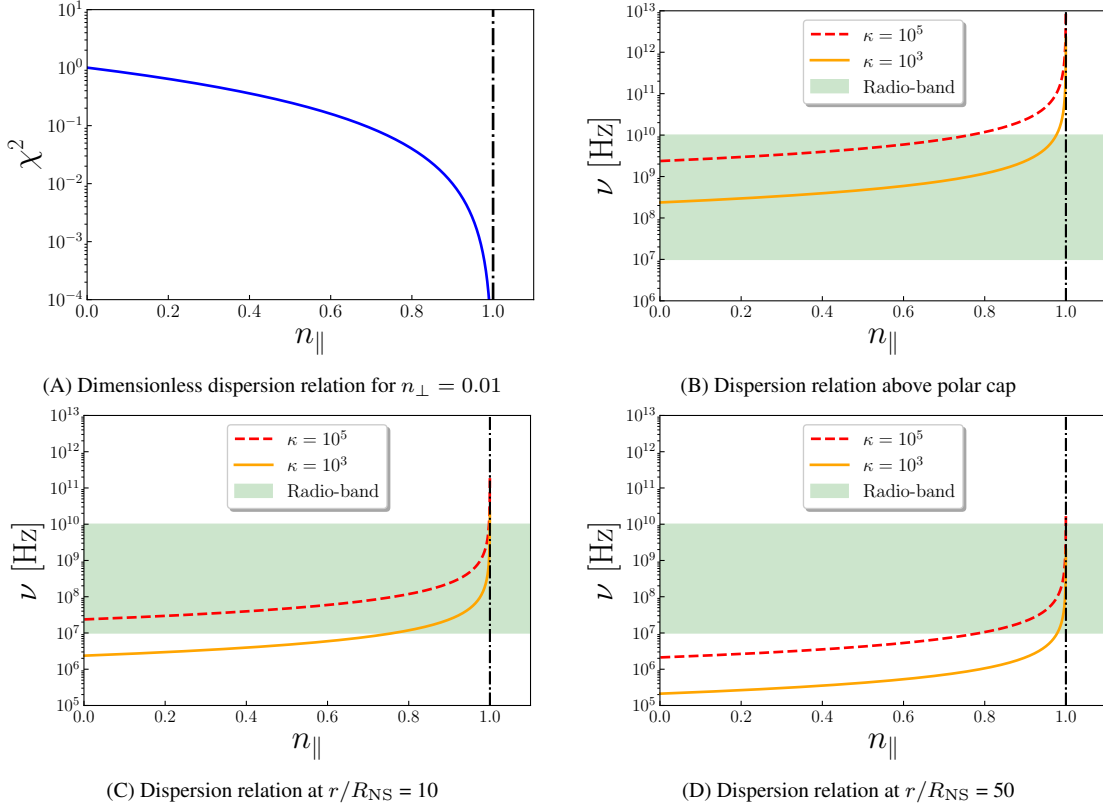


Figure 2. The figure shows the superluminal dispersion relation for bulk Lorentz factor $\gamma_s = 100$ at small angle of excitation ($n_\perp = 0.01$) and the radio-band (shown in light green) at various distances from the neutron star surface. The dot dashed black line in all panels shows the asymptotic refractive index of unity for superluminal lt_2 mode. The graphs are shown for the last open field line of an aligned rotator of period $P = 1$ sec and multiplicity $\kappa = 10^5$ (shown in dashed red line) and 10^3 (shown in solid yellow line). **Top:** Panel (A) shows the dimensionless dispersion relation for small angle of propagation ($n_\perp = 0.01$). Panel (B) shows that a major fraction of the radio-band occupies the stopband just above the polar cap for a highly non-dipolar surface magnetic field ($b = 10$). **Bottom:** Panel (C) shows that for $\kappa = 10^5$ even 100 km above the surface the frequencies below 50 MHz still occupies the stopband while frequencies up to 100 MHz lies close to the cut-off. Panel (D) shows that for $\kappa = 10^5$ only around 500 km above the surface the lt_2 dispersion relation describes the full radio-band. Both Panels (C) and (D) show that for $\kappa = 10^3$ the radio-band lies above the stopband even at distances of around 100 km above the neutron star surface.

$$\chi^2 = \frac{\omega_p^2}{\gamma_s^2 \omega^2} = \left(\frac{1 - n_\perp^2 - n_\parallel^2}{1 - n_\parallel^2} \right) (1 - n_\parallel \beta_o)^2 \quad (7)$$

where $\beta_o = v_o/c$. For the lt_2 mode n_\parallel and n_\perp are less than unity and further for small angle of excitation $n_\parallel \gg n_\perp$. For a given n_\perp , the parallel refractive index n_\parallel becomes the variable. It can be varied in the range $0 < n_\parallel < 1$. This gives χ^2 as a function of n_\parallel and is referred the dimensionless dispersion relation of the lt_2 mode. The χ^2 so obtained can be converted to the angular frequency (ω) using $\omega = \sqrt{\omega_p^2 / \chi^2 \gamma_s^3}$. This transformation gives ω as a function of n_\parallel to obtain the dispersion relation. It must be noted that for a given χ^2 and Lorentz factor γ_s , the angular frequency ω (where frequency $\nu = \omega/2\pi$) scales only as ω_p .

Fig. 2 shows the lt_2 dispersion relation assuming a stationary plasma flow. Panel (A) shows the dimensionless dispersion relation of the lt_2 mode for small angle excitation. Panels (B), (C) and (D) of Fig. 2 shows the dimensional lt_2 dispersion relation for $\kappa = 10^5$ (shown in dashed red) and $\kappa = 10^3$ (shown in solid yellow) for small ϑ . The $n_\parallel = 0$ in all the panels corresponds to the the cut-off frequency as defined in equation (5). For a constant $\gamma_s = 100$, the dispersion relation is solely a function of $\omega_p \propto \sqrt{\kappa}$. The lt_2 mode cannot admit travelling wave solutions below the cut-off frequency which represents the stopband. As seen from Panel (B) just above

the polar cap (with a strong non-dipolar magnetic field component) the lt_2 dispersion relation is valid for frequencies $\nu \gtrsim 2$ GHz for $\kappa = 10^5$ and $\nu \gtrsim 200$ MHz for $\kappa = 10^3$. Panel (C) shows that by around 100 km above the surface the full radio-band occupies the lt_2 dispersion relation for $\kappa = 10^3$ while frequencies below 50 MHz still occupies the stopband for $\kappa = 10^5$. Panel (D) shows that by 500 km from the surface the full radio-band overlaps with the lt_2 mode for both $\kappa = 10^3$ and $\kappa = 10^5$. Thus, just above the polar cap the range of frequencies admitted depends strongly on κ and by 500 km from the surface the full-radio band is admitted irrespective of κ . It must be noted that an increase in γ_s (not shown) also decreases the cut-off frequency. Thus, the full radio-band above polar cap can be accommodated by decreasing κ and increasing γ_s provided the plasma flow is stationary above the polar cap.

The ratio E_1/E_3 can be expressed as (see Eq. 22 of MMG14),

$$\frac{E_1}{E_3} = \frac{I \sin \vartheta \cos \vartheta}{I \sin^2 \vartheta - (1 - n^2)} \quad (8)$$

where

$$I = \chi^2 / (1 - n_\parallel \beta_o)^2 \quad (9)$$

Substituting $I = \chi^2 / (1 - n_\parallel \beta_o)^2$ from equation (9) and $n^2 =$

$n_{\parallel}^2 + n_{\perp}^2$ in equation (8) gives,

$$\frac{E_1}{E_3} = \frac{\chi^2 \sin \vartheta \cos \vartheta}{\chi^2 \sin^2 \vartheta - (1 - n_{\perp}^2 - n_{\parallel}^2)(1 - n_{\parallel} \beta_o)^2} \quad (10)$$

But, from the definition of χ^2 in equation (7) we have $(1 - n_{\perp}^2 - n_{\parallel}^2)(1 - n_{\parallel} \beta_o)^2 = \chi^2(1 - n_{\parallel}^2)$. This simplifies the expression above to

$$\frac{E_1}{E_3} = \frac{\sin \vartheta \cos \vartheta}{n_{\parallel}^2 - \cos^2 \vartheta} \quad (11)$$

Using equation (4) and equation (11) the ratio E_1/E_3 can be rewritten in the form

$$\frac{E_1}{E_3} = \tan \Theta = \frac{\sin \vartheta \cos \vartheta}{n_{\parallel}^2 - \cos^2 \vartheta} \quad (12)$$

Let Θ_{esc} be the angle that the wave electric field of the lt_2 mode makes with the wave vector \vec{k} at the escape point. At small ϑ from Table (2) we obtain the asymptotic parallel refractive index $n_{\parallel} \rightarrow \sqrt{1 - n_{\perp}^2} \rightarrow 1$ which when substituted in equation (12) gives,

$$\tan \Theta_{\text{esc}} = \lim_{n_{\parallel} \rightarrow 1} \frac{\sin \vartheta \cos \vartheta}{n_{\parallel}^2 - \cos^2 \vartheta} = \cot \vartheta \quad (13)$$

which gives

$$\Theta_{\text{esc}} \rightarrow \pi/2 - \vartheta \quad (14)$$

The equation (14) shows that the transverse character of the lt_2 mode increases for smaller ϑ .

It must also be noted that the components of lt_2 electric field parallel and perpendicular to the ambient magnetic field can be found using the following transformation

$$E_{\parallel} = E_3 \cos \vartheta + E_1 \sin \vartheta \quad (15)$$

$$E_{\perp} = -E_3 \sin \vartheta + E_1 \cos \vartheta \quad (16)$$

The condition for decoupling of the wave from plasma in strong magnetic field (i.e. charges confined to move in one dimension along magnetic field lines) requires $E_{\parallel} = 0$. Using $E_{\parallel} = 0$ in equation (15) gives,

$$\frac{E_1}{E_3} = -\cot \vartheta, \quad (17)$$

Using equation (17) in equation (8) and simplifying we get,

$$n^2 = (1 - 2I \sin^2 \vartheta) \quad (18)$$

The condition of decoupling must be simultaneous with the wave reaching vacuum-like propagation ($n = 1$). Substituting $n = 1$ and the expression for I gives

$$\left[\frac{\chi_{\text{decoup}}^2}{(1 - n_{\parallel} \beta_o)^2} \right] \sin^2 \vartheta \rightarrow 0 \quad (19)$$

For small $\vartheta \approx 1/\gamma_s$, we have $\sin \vartheta \approx \vartheta \approx 1/\gamma_s$ and $(1 - n_{\parallel} \beta_o) \approx (1 - \beta_o) \approx 1/\gamma_s(1 + \beta_o) \approx 1/2\gamma_s$. Using these simplifications and the expression of χ^2 from equation (7), the equation (19) reduces to the form,

$$\chi_{\text{decoup}}^2 = \frac{\omega_p^2}{\gamma_s^3 \omega_{\text{esc}}^2} = \frac{\omega_o^2}{\omega_{\text{esc}}^2} \rightarrow 0 \quad (20)$$

Thus, decoupling happens at very high frequencies ($\omega_{\text{esc}} \gg \omega_o$). Now, χ^2 at the characteristic plasma frequency ω_1 as defined in equation (6) is given by

$$\chi_{\omega_1}^2 \approx \frac{1}{\gamma_s^4} \geq \chi_{\text{decoup}}^2 \quad (21)$$

Comparing equation (20) and equation (21) we get,

$$\omega_{\text{esc}} \geq \omega_1 \quad (22)$$

Note the equality condition can be used only for large γ_s . At distances of 500 km from the surface using equation (1) and equation (6) we have $\omega_1 \sim 2 \times 10^{11}$ rad s⁻¹ for $\gamma_s = 100$. It implies that even in principle decoupling of lt_2 mode at around 500 km occurs at small ϑ for frequencies $\nu \gtrsim 30$ GHz for $\kappa = 10^5$.

The escape of the lt_2 wave requires the wave to acquire a transverse character in the plasma frame. It was shown by MMG14 (see their Eq. 26) that the lt_2 mode acquires almost an electromagnetic character i.e. $E_3 \rightarrow 0$ in the observer frame when the condition $\gamma_s \vartheta > 1$ is satisfied for $\omega \gtrsim \omega_1$. In order to understand the physical nature of this behaviour it is convenient and instructive to consider features of this wave in the plasma frame of reference. The plasma frame (referred to as the primed frame) moves with respect to the observers' frame (referred to as the unprimed frame) along the direction of the local magnetic field at the Lorentz factor γ_s . In the plasma frame the wave electric field components along and across the magnetic field can be described as

$$E'_1 = E'_{\parallel} \sin \vartheta' + E'_{\perp} \cos \vartheta' \quad (23)$$

$$E'_3 = E'_{\parallel} \cos \vartheta' - E'_{\perp} \sin \vartheta' \quad (24)$$

Here $\vartheta' = k'_{\perp}/k'_{\parallel}$ is the ratio of the wave vector components in the plasma frame. From the Lorentz transformation for the wave vector, it follows that $k_{\perp} = k'_{\perp}$ and $k_{\parallel} \approx \gamma_s k'_{\parallel}$, thus in the plasma frame $\vartheta' \approx \gamma_s \vartheta$ and using the condition $\gamma_s \vartheta > 1$, we get $\vartheta' > 1$. Similarly we can estimate the components of the electric field of a wave, as $E_{\parallel} = E'_{\parallel}$ and $E_{\perp} \simeq \gamma_s E'_{\perp}$, and hence the fulfilment of the condition $E_{\perp} \gg E_{\parallel}$ (i.e. the wave is almost transverse in the observers' frame) does not guarantee the fulfilment of the condition $E'_{\perp} \gg E'_{\parallel}$ (i.e. the wave is also almost transverse in the plasma frame). Indeed, estimations as in MMG14 show that $E_{\perp} \approx \gamma_s E_{\parallel}$, so it is clear from the equations that if ϑ' has an intermediate value between 0 and $\pi/2$, E'_1 and E'_3 should be the same order in the plasma frame. It must be noted that our analysis assumes a homogeneous plasma flow. The possibility of the escape of lt_2 waves under inhomogeneous plasma conditions requires further study and is outside the scope of this work.

3.2 Dependence of escape conditions on ϑ and κ

We have discussed above the escape conditions for small values of ϑ which is valid for dipolar magnetic field at the polar cap. However in the PTS20 mechanism this angle is measured between the normal to the pair production front (i.e. the direction of the wave vector) and the ambient magnetic field, and can, in general, vary by many orders of magnitude (up to ~ 1 radian), depending on the ambient magnetic field profile and on the shape of the pair production front. In the case of a highly non-dipolar surface field due to the small radius of curvature of the magnetic field lines the pair creation front can make large angle with respect to the global dipolar magnetic field axis. However in this case, the wave vector will not necessarily be directed along the open dipolar magnetic field lines but will propagate towards the close magnetic field line directions.

The presence of radio wave as traveling lt_2 mode in pulsar plasma also depends on the multiplicity κ . The characteristic frequency ω_1 can be lowered to occupy the radio-band if the density of the pair plasma decreases such that multiplicity $\kappa \leq 10^3$. In fact simulations suggests that during pair creation process only a small portion of the primary beam attains $\kappa \sim 10^5$, while the average multiplicity of

the trail has smaller values of $\kappa \sim 10^2 - 10^3$ (see e.g. Timokhin 2010), and hence there exist parameter space where lt_2 mode can have propagating solutions. However as we will discuss in section 4 an additional requirement to obtain valid traveling wave solutions for lt_2 mode is the presence of a stationary plasma is essential.

3.3 Constraints due to Group velocity

The energy pumped at a given angular frequency ω is transported at the the group velocity (\vec{v}_{gr}) of the lt_2 mode given by (see Appendix A)

$$\frac{1}{c} \vec{v}_{gr}(n_{\parallel}, n_{\perp}) = \beta_{gr,\parallel} \hat{b}_{\parallel} + \beta_{gr,\perp} \hat{b}_{\perp}$$

where b_{\parallel} and b_{\perp} are the unit vectors parallel and perpendicular to the ambient pulsar magnetic field respectively. Here, the components $\beta_{gr,\parallel}$ and $\beta_{gr,\perp}$ are given by

$$\beta_{gr,\parallel} = \frac{n_{\parallel} - \frac{n_{\parallel}^2 \chi^2}{(1-n_{\parallel}\beta_o)^2} + \frac{(1-n_{\parallel}^2)\chi^2 v_o}{(1-n_{\parallel}\beta_o)^3}}{\left\{ 1 - \frac{\chi^2}{(1-n_{\parallel}\beta_o)^2} \right\} + \frac{\chi^2(1-n_{\parallel}^2)}{(1-n_{\parallel}\beta_o)^3}} \quad (25)$$

$$\beta_{gr,\perp} = \frac{n_{\perp}}{\left\{ 1 - \frac{\chi^2}{(1-n_{\parallel}\beta_o)^2} \right\} + \frac{\chi^2(1-n_{\parallel}^2)}{(1-n_{\parallel}\beta_o)^3}} \quad (26)$$

Thus, the plasma waves propagate at an angle ϑ_{gr} to the local ambient magnetic field expressed as

$$\tan \vartheta_{gr} = \frac{\beta_{gr,\perp}}{\beta_{gr,\parallel}} \quad (27)$$

As discussed in the previous section, the pulsar magnetic field topology at the wave generation points is purely dipolar. The equation (27) shows that as a result of propagation the angle ϑ between the ambient magnetic field \vec{B} and the wave vector \vec{k} necessarily increases for a diverging set of magnetic field lines. Let ϑ_{gen} and ϑ_{esc} be the angle between the wave vector \vec{k} and \vec{B} at the generation point r_{gen} and the escape point respectively r_{esc} . Thus, if r_{gen} and r_{esc} are far away as a result of propagation we will have $\vartheta_{esc} \gg \vartheta_{gr} + \vartheta_{gen}$. As an illustrative example, consider r_{gen} and r_{esc} to be $\Delta r \sim 500$ km apart. The typical radius of curvature for magnetic field lines in the inner magnetosphere at radio emission heights is $\rho_c \sim 10^8$ cm. The change in angle $\Delta\vartheta$ between wave vector and the ambient magnetic field due to propagation gives $\Delta\vartheta \approx \Delta r / \rho_c \sim 0.5$ radians. Thus, even if ϑ_{gen} were to be small, propagation increases ϑ_{esc} . This violates the small angle approximation that is necessary for the plasma waves to acquire transverse character at r_{esc} . To prevent this situation the underlying emission mechanism must ensure that the plasma waves are generated very close to the escape point. This requires that the general class of lt_2 models must have a local character.

The limiting behavior of the properties of the lt_2 waves for small angle of excitation at the cut-off frequency ω_o and the characteristic frequency ω_1 are summarized in Table 2.

4 VALIDITY OF DISPERSION RELATION FOR EXTERNALLY DRIVEN MODEL OF RADIO EMISSION

As a particular example of an externally driven mechanism that can excite lt_2 mode, we consider the recent mechanism by PTS20. The

model appeals to the direct energy transfer from the transient electromagnetic field in the polar cap to the lt_2 mode due to a time-dependent gap screening process. The mechanism works as follows. During the pair cascade in the polar gap, the number density $n_s(t)$ of the pair plasma changes. As a result, a time-dependent plasma frequency $\omega_p(t) \propto \sqrt{n_p(t)}$ can be associated with the pair plasma. PTS20 suggests that energy associated with the transient external electromagnetic field at the polar gap is pumped at the time-dependent cut-off frequency $\omega_o(t) \propto \omega_p(t)$. In the time interval ($0 < t < t_{max}$) the cut-off frequency $\omega_o(t)$ spans the full radio band (roughly $\nu \sim 10$ MHz to 10 GHz).

While the suggestion of PTS20 is attractive, it is important to assess if the electromagnetic radiation that is produced due to the rapidly varying pair creation process can couple to the eigen modes of the relativistically streaming pulsar plasma. To investigate this let us briefly recall the non-stationary pair creation process above the polar cap as described in the inner vacuum gap models (Sturrock 1971; Ruderman & Sutherland 1975; hereafter RS75). The process starts when a high energy gamma ray photon traverses a mean free path distance of about h_g before it gets converted into an electron positron due to the presence of strong magnetic field above the polar cap. RS75 pointed out that this condition requires the h_g to be similar to the size of polar cap radius $h_g \approx r_{pc}$. For a purely dipolar surface geometry, $r_{pc,dip} \approx 100$ metres for a pulsar with $P = 1$ seconds. For the non-dipolar surface geometry, the polar cap radius $r_{pc,non-dip} = r_{pc,dip} / \sqrt{b} \sim 30$ meters using $b = 10$. Using $h_g \approx r_{pc,non-dip} \sim 30$ meters. RS75 suggested that the typical timescale τ associated with pair creation to be the light crossing time associated with h_g . Thus, τ is given by

$$\tau \sim h_g / c = 100 \text{ ns} = 10^{-7} \text{ s} \quad (28)$$

The pair creation process then undergoes a cascade until the induced electric field above the polar cap is screened completely, which happens in a time $t \approx 30 - 40\tau$ (see RS75). The numerical simulations of Timokhin (2010) have confirmed the same. Thus, the maximum time of discharge can be taken to be,

$$t_{max} \sim 40\tau = 4000 \text{ nanoseconds} \quad (29)$$

So, in a maximum time $t_{max} \approx 4000$ nanoseconds a dense pair plasma can be produced above the polar cap having number density corresponding to,

$$n_{s,max}(t = t_{max}) = \kappa \frac{bB_d}{Pce} \approx 10^{17} \left(\frac{1 \text{ s}}{P} \right) \left(\frac{B_d}{10^{12} \text{ G}} \right) \left(\frac{b}{10} \right) \left(\frac{\kappa}{10^5} \right) \text{ cm}^{-3} \quad (30)$$

The excited frequency ω at any time t can be represented as

$$\omega(t) = \omega_o(t) = a \sqrt{\left(\frac{n_s(t)}{\text{cm}^{-3}} \right)} \quad (31)$$

where a is a constant expressed as

$$a = \sqrt{\frac{4\pi e^2}{m_e} \frac{1}{\gamma_s^3}} \approx 56 \sqrt{\left(\frac{10^2}{\gamma_s} \right)^3} \text{ rad s}^{-1} \quad (32)$$

It must be noted that after a pair plasma discharge is complete (i.e., the plasma settles to a stable flow), the final cut-off frequency $\omega_{max} = \omega_o(t = t_{max})$ of the lt_2 mode is given by

$$\omega_{max} \approx 10^{10} \sqrt{\left(\frac{1 \text{ s}}{P} \right) \left(\frac{10^2}{\gamma_s} \right)^3 \left(\frac{\kappa}{10^5} \right) \left(\frac{B_d}{10^{12} \text{ G}} \right) \left(\frac{b}{10} \right)} \text{ rad s}^{-1}$$

(33)

From panel (B) of Fig. 2 it can be seen that the lower frequencies $\omega < \omega_{\max}$ occupies the stop-band of the lt_2 dispersion relation. The lt_2 mode cannot exist in the stop-band. The higher frequencies $\omega > \omega_{\max}$ cannot be excited as the proposed mechanism pumps energy only nearer the dynamic cut-off $\omega_o(t)$. As a result, the higher radio frequencies remain inaccessible to the direct energy transfer. Thus, the external energy transfer during gap discharge cannot excite lt_2 mode at radio frequencies to the plasma. Next we consider in detail as to why the notion of plasma wave solutions at broadband radio frequencies remains invalid for rapid pair cascade processes above polar cap.

Using equation (31) the change of the excitation frequency (ω) is governed by the equation

$$\frac{d\omega}{dt} = a \frac{d}{dt} \sqrt{n_s(t)} \quad (34)$$

The oscillation period (\mathcal{T}) associated with frequency ω is given by

$$\mathcal{T} = \frac{1}{2\pi\omega} \quad (35)$$

We now track the cascade process by slicing the total discharge time into smaller discrete time intervals Δt . The number density of the pair plasma can be assumed to be constant within Δt . The frequency of excitation changes by a fixed and small $\Delta\omega$ in each time interval (Δt). We assume that in the time interval Δt the plasma frequency ν_p changes by $\Delta\nu = 1$ MHz viz., a small fraction of the lowest observed radio frequency $\nu_{\text{low}} = 10$ MHz. This gives us the corresponding angular frequency $\Delta\omega$,

$$\Delta\omega = 2\pi\Delta\nu \approx 10^7 \text{ rad s}^{-1}, \quad (36)$$

A plasma wave of frequency ω must have sufficient number of oscillations within Δt . Using equation (35) this condition can be represented as,

$$\frac{\Delta t}{\mathcal{T}} = 2\pi\omega\Delta t \gg 1, \quad (37)$$

A plasma wave can be said to be excited only if the above condition holds. In what follows we consider two models of plasma discharge and check for the validity of equation (37). The models are a linear and an exponential plasma injection model.

In the linear model, the number density of the pair plasma increases linearly with time. This model is used in the recent study by PTS20. The pair plasma particles are injected at a constant rate \dot{n} . The number density of pair particles changes as

$$n_s(t) = \dot{n}t \quad \text{For } 0 < t < t_{\max} \quad (38)$$

The constant injection rate can be estimated using $t_{\max} = 40\tau$ from equation (29) and using $n_{s,\max}$ from equation (30) as

$$\dot{n} = \frac{n_{s,\max}}{t_{\max}} \approx 2.5 \times 10^{23} \left(\frac{10^{-7} \text{ s}}{\tau} \right) \left(\frac{\kappa}{10^5} \right) \left(\frac{b}{10} \right) \left(\frac{B_d}{10^{12} \text{ G}} \right) \left(\frac{1 \text{ s}}{P} \right) \text{ cm}^{-3} \text{ s}^{-1} \quad (39)$$

Substituting equation (38) into equation (34) gives

$$\Delta t = \frac{2\omega\Delta\omega}{a^2\dot{n}} \quad (40)$$

Substituting the above expression for Δt into equation (37) and then

using the value of a from equation (32) and the value of \dot{n} from equation (39) we get,

$$\omega^2 \Delta\omega \gg 10^{25} \left(\frac{10^{-7} \text{ s}}{\tau} \right) \left(\frac{\kappa}{10^5} \right) \left(\frac{b}{10} \right) \left(\frac{B_d}{10^{12} \text{ G}} \right) \left(\frac{10^2}{\gamma_s} \right)^3 \left(\frac{1 \text{ s}}{P} \right) \text{ rad}^3 \text{ s}^{-3} \quad (41)$$

The equation above shows that the largest number of oscillations can be accommodated for $\omega = \omega_{\max}$. Using the expression for ω_{\max} from equation (33) in equation (41), it can be seen that $\omega_{\max}^2 \Delta\omega \approx 10^{27} \text{ rad}^3 \text{ s}^{-3}$ such that the dependence on κ and γ_s vanishes and about hundred temporal oscillations can be accommodated.

The second model is a more realistic model, where the number density of the pair plasma increases exponentially (Sturrock 1971 ; Ruderman & Sutherland 1975 ; Hibschan & Arons 2001; Arendt & Eilek 2002). The number density of pair plasma can be modelled as

$$n_s(t) = \exp(t/\tau) \quad \text{For } 0 < t < t_{\max} \quad (42)$$

Substituting equation (42) in equation (34) gives

$$\Delta t = \frac{2\tau\Delta\omega}{\omega} \quad (43)$$

Substituting the above expression for Δt into equation (37) gives

$$4\pi\Delta\omega \tau \gg 1 \quad (44)$$

From equation (28) we estimate $\tau \sim 10^{-7}$ seconds, and it can be seen that in the exponential model up to ten temporal oscillations can be completely fulfilled across the full broad-band radio frequencies.

It must be noted that in the exponential model the condition (37) for the validity of travelling wave solution as expressed in equation (44) does not depend on κ or γ_s . Physically, it can be understood as follows: In the exponential model plasma number density increases e-fold after each characteristic timescale τ . Thus, the timescale Δt can only be a tiny fraction of the characteristic timescale τ as shown in equation (43).

It must also be mentioned during discharge the spatial scale $l = c\Delta t$ must be able to accommodate several ($\mathcal{N} \gg 1$) wavelengths λ for a plane travelling wave solution such that

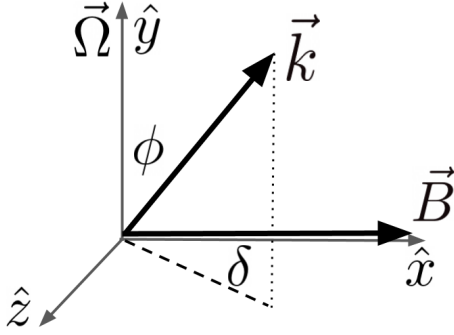
$$\mathcal{N} = \frac{c\Delta t}{\lambda} = \frac{1}{2\pi} n\omega\Delta t \quad (45)$$

Using equation (43) we have $\omega\Delta t = 2\tau\Delta\omega$. Using $\tau = 10^{-7}$ seconds from equation (28) and $\Delta\omega = 10^7 \text{ rad s}^{-1}$ from equation (36) we obtain the value $2\tau\Delta\omega = 2$. This value when substituted in equation (45) gives,

$$\mathcal{N} = \frac{n}{\pi} \left(\frac{\tau}{100 \text{ ns}} \right) \approx 0.32 n \left(\frac{\tau}{10^{-7} \text{ s}} \right) \quad (46)$$

The refractive index for the lt_2 mode is $n = ck/\omega < 1$ and closer to the dynamic cut-off $n \rightarrow n_{\perp}$. The lt_2 dispersion relation requires $n_{\perp} < 1$. Thus, irrespective of n_{\perp} (and hence ϑ) the dynamic scale l can hardly accommodate one wavelength across the entirety of the discharge process.

Thus, during pair plasma discharge plasma waves at radio frequencies cannot be generated. It is because the time interval for which plasma density can be assumed to be constant is too short to accommodate many oscillations (temporal and spatial) as is necessary for travelling plasma wave solutions to exist. Physically, the description of normal modes in a plasma is only possible when the plasma has settled to a stable state during which plasma frequency is constant. The stable state plasma supports eigen modes and admits



[h]

Figure 3. The figure shows the orthogonal co-ordinate system associated with the magnetic field plane. The $\hat{x}, \hat{y}, \hat{z}$ are the orthogonal unit vectors associated with the co-ordinate system. The $x - y$ plane corresponds to the magnetic field plane such that the rotation axis $\vec{\Omega}$ is along the y -axis while the ambient magnetic field \vec{B} is along x -axis. The wave vector \vec{k} makes an angle ϕ with the y -axis and the projection of \vec{k} on $x - z$ plane makes an angle δ with the x axis.

travelling wave solutions. The solutions at short times are referred to as transients. As discussed above, for very rapidly changing number density model the very notion of oscillatory plasma wave solutions remains inapplicable, and hence the electromagnetic waves found in the simulation of PTS20 cannot be identified as the eigen modes of the pair plasma. The total energy in the plasma is divided into the kinetic energy of the plasma particles and the normal modes of plasma oscillations. The energy pumped during the transient discharge phases can increase only the “temperature” (kinetic spread of the plasma distribution function) of the pair plasma. It is worth mentioning that the arguments presented in this section are not relevant for the externally rotation-driven pulsar emission mechanism studied by Melrose et al. (2021).

To summarize, the time-dependent pair discharge process at the polar gap cannot pump energy into lt_2 mode at radio frequencies. Any energy transfer during screening can only increase the momentum spread of the particle distribution function. The full radio-band can satisfy the lt_2 plasma dispersion relation only at few hundreds of km away from the surface (see Fig. 2). It is at these distances that the lt_2 mode can be excited in principle. However, it was shown in the previous section that at these heights the lt_2 waves cannot decouple from the plasma at radio frequencies. Only the t -mode can decouple from the plasma at the radio emission zone. In the next section we consider a fictitious mechanism that can excite t waves and analyse how the escape conditions dictates the orientation of the escaping waves with respect to the curved magnetic field lines.

5 ORIENTATION OF t -MODE AT THE DECOUPLING ZONE

In section 4 we argued that the electromagnetic waves generated due to the time-dependent pair creation process above polar cap cannot couple to the plasma eigen modes. Further as discussed in subsection 3.1, we have argued using general arguments that the lt mode cannot easily escape the plasma. Only the extra-ordinary t mode can escape from the homogeneous plasma. Here we consider a fictitious emission mechanism which can excite t mode in pair plasma. As mentioned in section 2 an important observational requirement for the escaping wave to be a candidate for pulsar radio emission is that

the linear polarization of the emerging radiation has to be parallel or perpendicular to magnetic field line planes. A further requirement is that the emission mechanism should be able to produce very highly linearly polarized (close to 100%) subpulses that follow the RVM. Hence our aim is to verify that if a fictitious emission mechanism that excites the t mode can be a candidate for pulsar radio emission. The first observational constraint requires us to find the direction of the excited wave with respect to magnetic field line planes and the second one requires to specify an averaging process that does not lead to significant depolarization.

Let us note that at about 10% of the light cylinder radius, where radio emission detaches from the pulsar magnetosphere, the radius of curvature of dipolar field lines are significantly larger than the wavelength of radio waves. This allows us to introduce a local cartesian co-ordinate system for the magnetic field plane as shown in Fig. 3. In this representation the ambient magnetic field \vec{B} , the wave vector \vec{k} and the wave electric field (\vec{E}_2) of the t -mode are given by

$$\vec{B} = B \hat{x} \quad (47)$$

$$\vec{E}_2 = E_{2x} \hat{x} + E_{2y} \hat{y} + E_{2z} \hat{z} \quad (48)$$

$$\vec{k} = k_x \hat{x} + k_y \hat{y} + k_z \hat{z} \quad (49)$$

Since for the t -mode \vec{E}_2 is perpendicular to the $k - B$ plane, the following two conditions must be satisfied

$$\vec{E}_2 \cdot \vec{B} = E_{\parallel} = 0 \quad (50)$$

$$\vec{E}_2 \cdot \vec{k} = 0 \quad (51)$$

Using equation (47) and equation (48) in equation (50) we get,

$$E_{2x} = 0$$

Using the result above, the wave electric E_2 can be represented as

$$\vec{E}_2 = E_{2y} \hat{y} + E_{2z} \hat{z} \quad (52)$$

Using equation (49) and equation (52) in equation (51) we have,

$$\frac{E_{2y}}{E_{2z}} = -\frac{k_z}{k_y} \quad (53)$$

From Fig. 3 the components of the wave vector (\vec{k}) can be represented as

$$k_y = k \cos \phi \quad (54)$$

$$k_x = k \sin \phi \cos \delta \quad (55)$$

$$k_z = k \sin \phi \sin \delta \quad (56)$$

Substituting equation (54) and equation (56) in equation (53) we define a dimensionless quantity ξ given by,

$$\xi = \frac{E_{2y}}{E_{2z}} = -\tan \phi \sin \delta \quad (57)$$

where E_{2y} and E_{2z} are the component of the wave electric field in the magnetic field plane and perpendicular to it. It must be noted that the angles ϕ and δ cannot vary independently. For a fixed angle of excitation ϑ between \vec{k} and \vec{B} , the dot product $\vec{k} \cdot \vec{B}$ must remain constant. This requires,

$$\cos \vartheta = \sin \phi \cos \delta = \text{constant} \quad (58)$$

which shows that many pairs of (ϕ, δ) can satisfy the relations above. However, for non-zero ϑ the pairs $(\phi = 0, \delta)$ and $(\phi, \delta = \pi/2)$ are excluded. Physically, this means that the wave vector \vec{k} can trace a cone with opening angle (ϑ) centred on the ambient magnetic field \vec{B} .

Now our objective is to find the condition under which we can

observe very high linear polarization of subpulses that follow the RVM in the pulsar radio emission zone (Mitra et al. 2009). The typical angular width of a subpulse is around $\sim 3^\circ \sim 6 \times 10^{-2}$ radians. For a bulk plasma flow with $\gamma_s = 100$, the typical emission cone due to any fictitious flow emission mechanism has opening angle $\vartheta \sim 1/\gamma_s \sim 10^{-2}$ radians. As the observer samples a subpulse the net emission at any point is an incoherent superposition of the electric field due to a large number of $1/\gamma_s$ emission cones that arises from nearby field lines. As discussed above, for generic fictitious mechanism(s) the electric field for an emission cone has no specific orientation with respect to the magnetic field plane. As a result, the incoherent averaging will necessarily lead to depolarization of the subpulse. In order to retain the high linear polarization the emission mechanism must preferentially select a fixed orientation of the t -mode electric field within $1/\gamma_s$ emission cones. Further, observations suggest that the emerging radio waves are polarized perpendicular to the magnetic field line planes (see e.g. Lai et al. 2001). The only known mechanism that can distinguish between the directions parallel and perpendicular to the magnetic field planes is the CCR.

It must be mentioned that studies like that of Cheng & Ruderman 1979 (hereafter CR79) suggest that due to propagation effects like adiabatic walking, close to 100 % linearly polarized subpulse can emerge at the escape region even if the polarization were to be random at the generation point. Adiabatic walking is a geometrical effect that requires the emission cones to move away from the curved magnetic field lines as a result of a rectilinear propagation. The particular condition required is that the emission must be at the characteristic plasma frequency ω_1 (see Eq. 7 of CR79). MMG14 showed that this condition does not hold at the radio emission zones. The radio emission is excited and escapes at frequencies much lower than the characteristic plasma frequency ω_1 of the outflowing plasma at distances of around 500 km from the surface. Hence the origin of highly linearly polarized subpulses cannot arise due to the mechanism suggested by CR79.

Considering CCR as the radio emission mechanism, we estimate the typical value of ξ for the escaping t -waves in the CCR regime ($\omega_{\text{CCR}} \ll \omega_1$), using the formalism of Gil et al. 2004 (hereafter GLM04) as shown in Appendix B. ξ_{CCR} for t -mode in the radiation zone is,

$$\xi_{\text{CCR}} \approx \gamma_s \gg 1 \quad (59)$$

Thus, CCR excites t waves that can freely escape from curved magnetic field lines with the predominant component of the wave electric field being perpendicular to the magnetic field planes at the radio emission zone. This corresponds to the case where $k - B$ planes coincides with the magnetic field planes.

It must be mentioned that the power in CCR is given in the X-mode perpendicular to the magnetic field plane and O-mode in the magnetic field plane. However, the power in O-mode of CCR is Razin suppressed for the lt_2 mode and is ducted along the magnetic field lines for lt_1 mode until it decays by Landau damping (Arons & Barnard 1986). It is the power in the X-mode that escapes as t waves. But, observations show the presence of a secondary polarization mode. It is identified with the O-mode. The escape of O-mode from pulsar plasma presents a problem for CCR regime. MMG14 has suggested that plasma density gradients can aid in the escape of lt modes. However, such studies that conclusively shows this effect are yet to be carried out. Secondly, the t mode and lt modes are linearly polarized. It is difficult to explain the origin of circular polarization in the CCR regime. Studies like Lyubarskii & Petrova (1998) have suggested a rotation induced coupling between the linearly polarized eigen modes can result in circular polarization. How-

ever, the effect of this coupling in the CCR regime still needs to be investigated.

To summarize, while the t mode can freely escape the plasma, any fictitious mechanism cannot explain the observational features. Only t mode excited by CCR can explain certain key observational features like close to 100% polarization of sub-pulses that follow the RVM and the observed perpendicular orientation of the electric field with respect to the magnetic field line planes. However, the origin of OPMs and circular polarization in CCR regime still remains unresolved.

6 CONCLUSION

In this study we obtain constraints on the externally driven plasma model of PTS20, that has been proposed to excite superluminal lt_2 mode as a candidate for explaining pulsar radio emission. The model considers the time dependent pair creation process at the polar cap as a source of electromagnetic radiation which can directly transfer energy to superluminal lt_2 mode at a small angle of excitation. However, for realistic pulsar parameters (see section 2) we find that the notion of traveling-wave solutions is not suitable for both linear and exponential models of pair cascade discharge just above polar cap irrespective of the value of plasma multiplicity κ and the bulk Lorentz factor γ_s . We suggest that any transient energy exchanges during discharge can only be channelled into increasing the momentum spread of the pair plasma particles. It must be noted here that the pair cascade model fails because the associated characteristic timescale τ is very small ~ 100 nanoseconds. In the vacuum gap models, the characteristic timescale τ is of the order of light crossing time of the polar cap radius and hence cannot be changed drastically. However, after the discharge when a stationary plasma flow is established, fictitious mechanisms operating on much longer timescales compared to timescale τ are not ruled out (see e.g. Melrose et al. 2021). As discussed in subsection 3.1 the dispersion relation of lt_2 mode at radio frequencies changes with plasma multiplicity κ and the bulk Lorentz factor γ_s . The lt_2 dispersion relation allows travelling-wave solutions for frequencies only above the cut-off frequency $\omega_o \propto \sqrt{\kappa}/\gamma_s^{3/2}$. For a constant γ_s , the cut-off frequency ω_o is higher for higher multiplicity and vice versa. As a result, the lt_2 dispersion relation spans the full broadband radio frequencies closer to the neutron star for lower multiplicities and farther away from the neutron star for higher multiplicities. This effect is shown in Fig. 2 where for a constant $\gamma_s = 100$, the full broad-band radio frequencies are spanned a few tens of km and a few hundreds of km above the surface for $\kappa = 10^3$ and $\kappa = 10^5$ respectively. It must also be noted for a fixed κ , decreasing the bulk Lorentz factor γ_s increases the cut-off frequency ω_o thereby increasing the distance where the full radio-band can be spanned. Thus, for any fictitious emission mechanism traveling wave solutions are possible in regions where the full radio-band can be accommodated. However even if the radio-band can be excited at these regions, we find that the lt_2 modes cannot escape from the plasma under homogeneous conditions.

The only mode that can freely escape the plasma is the t mode. However, we show that for an arbitrary fictitious mechanism the emergent polarization of the wave is randomly oriented with respect to the magnetic field line planes. Averaging of such random polarization inevitably leads to depolarization of the signal which is in contradiction with observations where 100% polarized subpulses are seen that follow the RVM. However, CCR can excite the plasma modes both parallel and perpendicular to the field line planes. As a result, the emerging t mode excited due to CCR can

have polarization perpendicular to magnetic field planes. This aspect is consistent with observations, and to the best of our knowledge, no other known mechanism(s) satisfies these stringent constraints. Hence CCR seems not only viable but a very promising alternative.

ACKNOWLEDGEMENTS

We thank the anonymous referee for critical comments and suggestions that has greatly improved the quality of the manuscript. We thank Rahul Basu for discussions and critical comments on the manuscript. Sk. MR and DM acknowledge the support of the Department of Atomic Energy, Government of India, under project no. 12-R&D-TFR-5.02-0700. DM acknowledges support and funding from the ‘Indo-French Centre for the Promotion of Advanced Research - CEFIPRA’ grant IFC/F5904-B/2018. This work was supported by the grant 2020/37/B/ST9/02215 of the National Science Centre, Poland.

DATA AVAILABILITY

No new data were generated or analysed in support of this research.

REFERENCES

- Arendt Paul N. J., Eilek J. A., 2002, *ApJ*, **581**, 451
Arons J., Barnard J. J., 1986, *ApJ*, **302**, 120
Arumugasamy P., Mitra D., 2019, *MNRAS*, **489**, 4589
Asseo E., Melikidze G. I., 1998, *MNRAS*, **301**, 59
Basu R., Mitra D., Melikidze G. I., 2020, *MNRAS*, **496**, 465
Blasi P., Amato E., 2011, *Astrophysics and Space Science Proceedings*, **21**, 624
Blaskiewicz M., Cordes J. M., Wasserman I., 1991, *ApJ*, **370**, 643
Cheng A. F., Ruderman M. A., 1979, *ApJ*, **229**, 348
Cruz F., Grismayer T., Chen A. Y., Spitkovsky A., Silva L. O., 2021, arXiv e-prints, p. [arXiv:2108.11702](https://arxiv.org/abs/2108.11702)
Force M. M., Demorest P., Rankin J. M., 2015, *MNRAS*, **453**, 4485
Geppert U., 2017, *Journal of Astrophysics and Astronomy*, **38**, 46
Gil J., Mitra D., 2001, *ApJ*, **550**, 383
Gil J. A., Melikidze G. I., Mitra D., 2002, *A&A*, **388**, 235
Gil J., Lyubarsky Y., Melikidze G. I., 2004, *ApJ*, **600**, 872
Ginzburg V. L., Zhelezniakov V. V., 1975, *ARA&A*, **13**, 511
Goldreich P., Julian W. H., 1969, *ApJ*, **157**, 869
Hardee P. E., Rose W. K., 1978, *ApJ*, **219**, 274
Hibschman J. A., Arons J., 2001, *ApJ*, **560**, 871
Jackson J. D., 1999, *Classical electrodynamics*, 3rd ed. edn. Wiley, New York, NY, <http://cdsweb.cern.ch/record/490457>
Johnston S., Hobbs G., Vigeland S., Kramer M., Weisberg J. M., Lyne A. G., 2005, *MNRAS*, **364**, 1397
Kazbegi A. Z., Machabeli G. Z., Melikidze G. I., 1991, *MNRAS*, **253**, 377
Lai D., Chernoff D. F., Cordes J. M., 2001, *ApJ*, **549**, 1111
Lakoba T., Mitra D., Melikidze G., 2018, *MNRAS*, **480**, 4526
Lyubarskii Y. E., Petrova S. A., 1998, *Ap&SS*, **262**, 379
Lyutikov M., Blandford R. D., Machabeli G., 1999, *MNRAS*, **305**, 338
Medin Z., Lai D., 2007, *MNRAS*, **382**, 1833
Melikidze G. I., Gil J. A., Pataraya A. D., 2000, *ApJ*, **544**, 1081
Melikidze G. I., Mitra D., Gil J., 2014, *ApJ*, **794**, 105
Melrose D. B., 1995, *Journal of Astrophysics and Astronomy*, **16**, 137
Melrose D. B., Rafat M. Z., Mastrano A., 2021, *MNRAS*, **500**, 4549
Mitra D., 2017, *Journal of Astrophysics and Astronomy*, **38**, 52
Mitra D., Li X. H., 2004, *A&A*, **421**, 215
Mitra D., Gil J., Melikidze G. I., 2009, *ApJ*, **696**, L141
Mitra D., Basu R., Melikidze G. I., Arjunwadkar M., 2020, *MNRAS*, **492**, 2468

- Noutsos A., Kramer M., Carr P., Johnston S., 2012, *MNRAS*, **423**, 2736
Noutsos A., Schnitzeler D. H. F. M., Keane E. F., Kramer M., Johnston S., 2013, *MNRAS*, **430**, 2281
Pétri J., Mitra D., 2020, *MNRAS*, **491**, 80
Philippov A., Timokhin A., Spitkovsky A., 2020, *Phys. Rev. Lett.*, **124**, 245101
Radhakrishnan V., Cooke D. J., 1969, *Astrophys. Lett.*, **3**, 225
Rahaman S. M., Mitra D., Melikidze G. I., 2020, *MNRAS*, **497**, 3953
Rankin J. M., 2015, *ApJ*, **804**, 112
Riley T. E., et al., 2019, *ApJ*, **887**, L21
Ruderman M. A., Sutherland P. G., 1975, *ApJ*, **196**, 51
Shapakhidze D., Machabeli G., Melikidze G., Khechinashvili D., 2003, *Phys. Rev. E*, **67**, 026407
Sturrock P. A., 1971, *ApJ*, **164**, 529
Szary A., Melikidze G. I., Gil J., 2015, *MNRAS*, **447**, 2295
Szary A., Gil J., Zhang B., Haberl F., Melikidze G. I., Geppert U., Mitra D., Xu R.-X., 2017, *ApJ*, **835**, 178
Timokhin A. N., 2010, *MNRAS*, **408**, 2092
Timokhin A. N., Harding A. K., 2019, *ApJ*, **871**, 12
Weltevrede P., Johnston S., 2008, *MNRAS*, **391**, 1210
Young M. D., Manchester R. N., Johnston S., 1999, *Nature*, **400**, 848
de Jager O. C., 2007, *ApJ*, **658**, 1177
von Hoensbroech A., Xilouris K. M., 1997, *A&A*, **324**, 981

APPENDIX A: GROUP VELOCITY OF lt_2 MODE

For simplicity we assume $c = 1$. The dispersion relation of the lt_2 mode are

$$\epsilon(\omega, k_{\parallel}, k_{\perp}) = (\omega^2 - k_{\parallel}^2) \left[1 - \frac{\omega_p^2}{\gamma_o^3(\omega - k_{\parallel}v_o)^2} \right] - k_{\perp}^2 = 0 \quad (\text{A1})$$

The group velocity of the lt_2 mode are given by

$$\vec{v}_{\text{gr}} = \frac{\partial \omega}{\partial k_{\perp}} \hat{b}_{\perp} + \frac{\partial \omega}{\partial k_{\parallel}} \hat{b}_{\parallel} \quad (\text{A2})$$

where \hat{b}_{\parallel} and \hat{b}_{\perp} are unit vectors parallel and perpendicular to the ambient magnetic field \vec{B} .

Taking derivative of equation (A1) with respect to k_{\perp} we get

$$\frac{\partial \omega}{\partial k_{\perp}} \left[\left\{ 1 - \frac{\chi^2}{(1 - n_{\parallel}v_o)^2} \right\} + \frac{\chi^2(1 - n_{\parallel}^2)}{(1 - n_{\parallel}v_o)^3} \right] = n_{\perp} \quad (\text{A3})$$

Taking derivative of equation (A1) with respect to k_{\parallel} we get

$$\begin{aligned} \frac{\partial \omega}{\partial k_{\parallel}} \left[\left\{ 1 - \frac{\chi^2}{(1 - n_{\parallel}v_o)^2} \right\} + \frac{\chi^2(1 - n_{\parallel}^2)}{(1 - n_{\parallel}v_o)^3} \right] \\ = n_{\parallel} \left[\left\{ 1 - \frac{n_{\parallel}\chi^2}{(1 - n_{\parallel}v_o)^2} \right\} + \frac{(1 - n_{\parallel}^2)\chi^2v_o}{(1 - n_{\parallel}v_o)^3} \right] \end{aligned} \quad (\text{A4})$$

APPENDIX B: POLARIZATION OF t MODE FOR CCR IN THE RADIATION ZONE

We refer the reader to the cylindrical co-ordinate system (r, θ, z) GLM04 in fig. 1 in GLM04. The goal is to estimate the orientation of emergent electric field in the radiation zone $r \gg r_o$ due to t waves generated by CCR bunches located at $r \approx r_o$.

The wave vector has \vec{k} has the components (k_r, k_{θ}, k_z) while the wave electric field \vec{E}_{wave} has the components (E_r, E_{θ}, E_z) . The representation of the wave vector \vec{k} and the wave electric field are con-

nected to the local cartesian system of Fig. 3 by the transformation

$$k_{\parallel} = k_{\theta} \quad (\text{B1})$$

$$k_{\perp} = \sqrt{k_z^2 + k_r^2} \quad (\text{B2})$$

$$E_{\parallel} = E_{\theta} \quad (\text{B3})$$

$$E_{\perp} = \sqrt{E_z^2 + E_r^2} \quad (\text{B4})$$

GLM04 introduces the dimensionless variables s and x are defined for small angle propagation as

$$s = kr_{\circ} \quad (\text{B5})$$

$$x = \left(\frac{r-r_{\circ}}{r}\right) s^{2/3} \quad (\text{B6})$$

As per this definition $x s^{-2/3} \ll 1$ corresponds to the near-field and $x s^{-2/3} \gg 1$ corresponds to the radiation zone.

For the t mode we have $E_{\parallel} = E_{\theta} = 0$ which gives

$$\vec{E} = (E_r, 0, E_z) \quad (\text{B7})$$

The components E_r and E_z can be estimated from the vector potential $\vec{A}(A_r, A_{\theta}, 0)$ from (see Eq. 4 and 6 of GLM04)

$$E_r = ik_z A_{\rho} \quad (\text{B8})$$

$$E_z = -k \left(iA_{\theta} + s^{-1/3} \frac{\partial A_{\rho}}{\partial x} \right) \quad (\text{B9})$$

where the t mode dispersion relation $\omega/c = k$ has been used for simplification.

In the CCR regime, the following relationship holds among the vector potential (see Eq. 24 of GLM04)

$$A_{\theta} = -\frac{is^{1/3}}{2x} \frac{\partial A_r}{\partial x} \quad (\text{B10})$$

In the radiation zone the vector potential A_r has the asymptotic solution (see Eq. 26 of GLM04)

$$A_r = \exp\left(i\frac{2\sqrt{2}}{3}x^{3/2}\right) \quad (\text{B11})$$

Using equation (B11) in equation (B10) we get,

$$A_{\theta} = \frac{s^{1/3}}{\sqrt{2x}} \exp\left(i\frac{2\sqrt{2}}{3}x^{3/2}\right) \quad (\text{B12})$$

Using equation (B11) and equation (B10) in equation (B8) and equation (B9) gives us

$$E_z = -ik \left(\frac{s^{1/3} + 2xs^{-1/3}}{\sqrt{2x}} \right) \exp\left(i\frac{2\sqrt{2}}{3}x^{3/2}\right) \quad (\text{B13})$$

$$E_r = ik_z \exp\left(i\frac{2\sqrt{2}}{3}x^{3/2}\right) \quad (\text{B14})$$

In the radiation zone we have $x s^{-2/3} \gg 1$ which reduces the equation to

$$E_z = -ik\sqrt{2xs^{-2/3}} \exp\left(i\frac{2\sqrt{2}}{3}x^{3/2}\right) \quad (\text{B15})$$

$$E_r = ik_z \exp\left(i\frac{2\sqrt{2}}{3}x^{3/2}\right) \quad (\text{B16})$$

For CCR we have $k/k_z \approx \gamma_s$ and $s = \gamma_s^3$. We define a dimensionless quantity ξ_{CCR} in the radiation zone from equation (B15) and (B16) as

$$\xi_{\text{CCR}} = \left| \frac{E_z}{E_r} \right| \approx \sqrt{x} \quad (\text{B17})$$

In the radiation zone we have $x s^{-2/3} \gg 1$ which translates to the condition $x \gg s^{2/3}$. Using $s = \gamma_s^3$ we have $x \gg \gamma_s^2$. This condition reduces the equation above to the form

$$\xi_{\text{CCR}} = \left| \frac{E_z}{E_r} \right|_{\text{radiation-zone}} \gg \gamma_s \gg 1 \quad (\text{B18})$$

Thus, in the radiation zone the emergent radio waves due to t waves excited by CCR emerges predominantly polarized perpendicular to the magnetic field plane. It must be noted that the Eq. 18 of GLM04 represents the wave electric field in the near-field, i.e. $\xi_{\text{CCR, near-field}} = -s^{1/3}k/(k_z\sqrt{2x})$.

As a final check of consistency, we investigate whether the waves at the radiation zone can freely escape the plasma. To do so it is necessary that the waves in the radiation zone retain a transverse character while satisfying the small wavelength approximation (see Eq. B4 of GLM04) expressed as

$$k_r^2 \approx 2 \frac{s^{4/3}x}{r_{\circ}^2} \quad (\text{B19})$$

The transverse character of the emergent waves require ($\vec{k} \cdot \vec{E} = 0$)

$$k_r = -\left(\frac{E_z}{E_r}\right) k_z \quad (\text{B20})$$

By substituting equation (B16) and equation (B15) in equation (B20) we get,

$$k_r^2 = k_z^2 \left(\frac{E_z}{E_r}\right)^2 = k^2 2xs^{-2/3} = \frac{s^2}{r_{\circ}^2} 2xs^{-2/3} \quad (\text{B21})$$

Thus, the equality of the expression can be seen from comparing equation (B19) and equation (B20).

To summarize, t mode excited by CCR bunches can escape as freely propagating transverse electromagnetic radiation in the radiation zone such that the predominant component of the wave electric field is perpendicular to the magnetic field plane.

APPENDIX C: NOTATIONS AND SYMBOLS USED THROUGHOUT THE TEXT

- P : Period of pulsar.
- B_d : Strength of the global magnetic field of the pulsar.
- B_s : Strength of the non-dipolar surface magnetic field.
- b : Ratio of B_s to B_d at the neutron star surface.
- ρ_c : Radius of curvature of the magnetic field lines.
- n_{GJ} : Goldreich-Julian number density.
- κ : Multiplicity of pair plasma.
- n_s : Number density of pair plasma.
- γ_s : Bulk lorentz factor of the pair plasma.
- ω : The angular frequency of a plasma wave.
- k : The wave number of a plasma wave
- \vec{k} : wave vector of the plasma waves.
- \vec{B} : The local ambient pulsar magnetic field.
- $k-B$ plane: The plane containing \vec{k} and \vec{B} .
- ϑ : The angle between \vec{k} and \vec{B} as shown in Fig. 1. Referred to as angle of excitation.
- t -mode: The purely transverse mode perpendicular to the $k-B$ plane.
- ordinary lt mode: The longitudinal-transverse plasma mode confined to the $k-B$ plane.
- Langmuir L mode: The purely longitudinal and electrostatic ordinary mode for $\vartheta = 0$.
- TE -mode: The purely transverse lt mode for $\vartheta = \pi/2$.
- lt_1 waves: The subluminal branch of the lt mode for $\vartheta > 0$.
- lt_2 waves: The superluminal branch of the ordinary mode for $\vartheta > 0$.
- ω_p : The plasma frequency of the pair plasma as defined in equation (1).

- ω_o : The cut-off frequency of Langmuir mode and lt_2 waves defined in equation (5).
- ω_1 : The characteristic frequency of the plasma as defined in equation (6).
- \vec{E}_{wave} : The wave electric field of the lt_2 waves.
- \vec{E}_2 : The wave electric field of t wave perpendicular to the $k-B$ plane.
- E_1 : Projection of \vec{E}_{wave} perpendicular to \vec{k} .
- E_3 : Projection of \vec{E}_{wave} parallel to \vec{k} .
- E_\perp : Projection of \vec{E}_{wave} perpendicular to \vec{B} .
- E_\parallel : Projection of \vec{E}_{wave} parallel to \vec{B} .
- Θ : The angle between wave electric field \vec{E}_{wave} and \vec{k} as defined in equation (4).
- k_\perp : Projection of \vec{k} perpendicular to \vec{B} .
- k_\parallel : Projection of \vec{k} parallel to \vec{B} .
- $n = kc/\omega$: The refractive index of plasma for a plasma wave of frequency ω and wave number k .
- $n_\parallel = n \cos \vartheta$: parallel refractive index of the plasma.
- $n_\perp = n \sin \vartheta$: perpendicular refractive index of the plasma.
- \vec{v}_{gr} : The group velocity of lt_2 waves.
- ϑ_{gr} : Angle between the ambient magnetic field \vec{B} and group velocity \vec{v}_{gr} of the lt_2 mode as defined in equation (27).
- τ : The characteristic timescale associated with pair cascade process in the polar cap as defined in equation (28).
- t_{max} : The maximum timescale of discharge as defined in equation (29).
- $\vec{\Omega}$: Rotation vector of the pulsar.
- Magnetic field plane: The plane containing $\vec{\Omega}$ and \vec{B} as shown in Fig. 3.
- ϕ : The angle between \vec{k} and the rotation axis $\vec{\Omega}$ as shown in Fig. 3.
- δ : The angle between the projection of the wave vector on the plane perpendicular to the magnetic field plane and the ambient magnetic field \vec{B} as shown in Fig. 3.
- CCR: Coherent Curvature Radiation
- ξ_{CCR} : The ratio of t mode electric field parallel and perpendicular to the magnetic field plane as defined in equation (59).

This paper has been typeset from a $\text{\TeX}/\text{\LaTeX}$ file prepared by the author.